

OXFORD
UNIVERSITY PRESS

Human Molecular Genetics

Dominant and recessive mutations in rhodopsin activate different cell death pathways

Journal:	<i>Human Molecular Genetics</i>
Manuscript ID	HMG-2016-D-00174.R1
Manuscript Type:	2 General Article - UK Office
Date Submitted by the Author:	n/a
Complete List of Authors:	Comitato, Antonella; University of Modena, Department of Life Sciences Di Salvo, Maria Teresa; University of Modena, Department of Life Sciences Turchiano, Giandomenico; University of Modena, Department of Life Sciences Montanari, Monica; University of Modena, Department of Life Sciences Sakami, Sanae; Case Western University, Pharmacology Palczewski, Krzysztof; Case Western University, Pharmacology; Marigo, Valeria; University of Modena, Department of Life Sciences
Key Words:	retinitis pigmentosa, apoptosis, neuroprotection, rhodopsin

SCHOLARONE™
Manuscripts

Review

1
2
3 **Dominant and recessive mutations in rhodopsin activate different cell death**
4 **pathways**
5
6
7
8

9 Antonella Comitato¹, Maria Teresa Di Salvo¹, Giandomenico Turchiano^{1,§}, Monica
10 Montanari¹, Sanae Sakami², Krzysztof Palczewski², Valeria Marigo^{1,*}
11
12
13

14
15
16 ¹Department of Life Sciences, University of Modena and Reggio Emilia, 41125 Modena,
17 Italy
18

19
20 ²Department of Pharmacology, Cleveland Center for Membrane and Structural Biology,
21 School of Medicine, Case Western Reserve University, Cleveland, OH 44106, USA
22
23

24
25
26
27 [§]Current address: Institute for Cell and Gene Therapy & Center for Chronic
28 Immunodeficiency - University of Freiburg, Freiburg, Germany
29
30

31
32
33
34 ^{*}Corresponding Author: Valeria Marigo, Department of Life Sciences, University of Modena
35 and Reggio Emilia, via Campi, 287, 41125 Modena, Italy; phone: +390592055392; fax:
36 +390592055410; email: valeria.marigo@unimore.it
37
38
39
40
41
42
43
44
45
46
47
48
49
50
51
52
53
54
55
56
57
58
59
60

Abstract

1
2
3
4
5 Mutations in rhodopsin (RHO) are a common cause of retinal dystrophy and can be
6
7 transmitted by dominant or recessive inheritance. Clinical symptoms caused by dominant
8
9 and recessive mutations in patients and animal models are very similar but the molecular
10
11 mechanisms leading to retinal degeneration may differ. We characterized three murine
12
13 models of retina degeneration caused by either Rho loss of function or expression of the
14
15 P23H dominant mutation in Rho. Rho loss of function is characterized by activation of
16
17 calpains and apoptosis-inducing factor (Aif) in dying photoreceptors. Retinas bearing the
18
19 P23H dominant mutations activate both the calpain-Aif cell death pathway and ER-stress
20
21 responses that together contribute to photoreceptor cell demise. *In vivo* treatment with the
22
23 calpastatin peptide, a calpain inhibitor, was strongly neuroprotective in mice lacking Rho
24
25 while photoreceptor survival in retinas expressing the P23H dominant mutation was more
26
27 affected by treatment with salubrinal, an inhibitor of the ER-stress pathway. The further
28
29 reduction of photoreceptor cell demise by co-treatment with calpastatin and salubrinal
30
31 suggests co-activation of the calpain and ER-stress death pathways in mice bearing
32
33 dominant mutations in the *Rho* gene.
34
35
36
37
38
39
40
41
42
43
44
45
46
47
48
49
50
51
52
53
54
55
56
57
58
59
60

Introduction

Retinitis pigmentosa (RP) is an inherited form of retinal degeneration characterized by progressive loss of the peripheral visual field leading to tunnel vision and finally blindness. Patients experience difficulties with dark adaptation and night blindness in adolescence followed by loss of the mid-peripheral visual field in young adulthood (1). Visual symptoms mirror the progressive loss of rod photoreceptors. Causative mutations for RP have been identified in several genes (Retnet database: <http://www.sph.uth.tmc.edu/retnet>). These genes encode proteins with very diverse functions and patterns of expression, which can be restricted to rods or be expressed by several neurons in the human retina (<http://rpexp.tigem.it/>; (2)). Mutations in *Rhodopsin* (*RHO*) represent a common cause of RP, accounting for 25% of autosomal dominant RP (adRP) and 8 to 10% of all RP (1) with more than 100 different associated mutations identified so far (<http://www.hgmd.cf.ac.uk>). Impairment of the phototransduction cascade caused by *RHO* loss of function is linked to autosomal recessive Retinitis Pigmentosa (arRP) and congenital night blindness (CNB) (3, 4). The molecular mechanisms underlying cell death caused by either dominant or recessive mutations in *RHO* are still not well characterized.

RHO is a G-protein coupled receptor localized to rod outer segments where the phototransduction cascade is initiated. *RHO* is the most abundant protein produced by rod cells accounting for 30% of their total protein content and is particularly enriched, up to 90%, in the rod outer segments (5–7). Data regarding the pathogenic mechanism(s) of mutant *RHO* are still controversial. Accumulation of mutant *RHO* in different subcellular compartments, including the endoplasmic reticulum (ER), may trigger the unfolded protein response (UPR) with cytoprotective outputs that reduce protein synthesis and up-regulate chaperones to cope with stress (8). Excessive mutant *RHO* accumulation can then lead to ER-stress responses that culminate with cell death (9). **ER-stress and other mechanisms**

1
2
3 involving the ER-associated degradation (ERAD) pathway and autophagy have been
4
5 linked to RHO mutation and may all contribute to retinal degeneration (10, 11). Saliba and
6
7 colleagues reported that exposure of p.Pro23His (P23H) mutant RHO, the most common
8
9 mutation in USA (12), to 9-*cis*-retinal in transfected cells increased plasma membrane
10
11 localization of the mutant protein but did not decrease the formation of aggresomes or
12
13 their detrimental effects (13). Murine models to study effects caused by mutant RHO and
14
15 specifically the P23H mutation are available as transgenic mice and rats (14, 15) that
16
17 suffer a very severe form of retinal degeneration. More recently, two knock-in mouse
18
19 models were generated for the P23H mutation and they show a much slower progression
20
21 of the disease (16, 17).
22
23

24
25 Quality control during protein synthesis imposed by the ER activates ER resident
26
27 sensors involved in the UPR to allow only properly folded proteins to leave the organelle.
28
29 Expression of mutant proteins may affect cellular ability to cope with UPR causing the cell
30
31 to activate ER-stress and succumb to apoptosis. The transducers of the UPR/ER-stress
32
33 responses are ER resident proteins: the inositol-requiring enzyme 1 (Ire1), the activating
34
35 transcription factor-6 (Atf6) and the protein kinase R-like ER protein kinase (Perk). Ire1 is a
36
37 ribonuclease that, when activated, splices the mRNA encoding X-box transcription factor 1
38
39 (*Xbp1*), leading to a frame shift and production of sXbp1, a transcription factor regulating
40
41 expression of chaperones. The Perk pathway is characterized by phosphorylation of Perk
42
43 and eukaryotic initiation factor-2 α (eIF2 α) resulting in reduction of protein synthesis and
44
45 up-regulation of Atf4 that regulates expression of several cell death related genes (18).
46
47
48

49
50 We previously showed that calpain activation as well as nuclear translocation of Aif
51
52 (Apoptosis-inducing factor) play fundamental roles in photoreceptor cell death in the retinal
53
54 degeneration 1 (*rd1*) mouse model (19, 20). Aif is a mitochondrial protein that can be
55
56 cleaved by calpains, leaves the mitochondrion through a pore formed by Bax and recruits
57
58
59
60

1
2
3 Cyclophilin A for chromatin fragmentation (21, 22). Aif, as well as ER-stress, were reported
4
5 to be activated in P23H transgenic rodents (23–25).
6

7
8 In this study we characterized the interrelationship of these calpain-mediated and ER
9
10 stress-mediated cell death pathways in Rhodopsin mutant mice. Specifically, we compared
11
12 the Rho knock-out mouse, a model for arRP, with two lines of mice expressing P23H
13
14 mutant Rho, models for adRP. We isolated expression of the P23H mutation from wild
15
16 type Rho in one of the two models to uncover molecular cytotoxic mechanisms activated
17
18 by the dominant mutation. Co-expression of wild type Rho, in fact, alleviates the
19
20 phenotype and may hinder the characterization of molecular pathways (9). We
21
22 characterized the different contributions of the two pathways by *in vivo* treatments with
23
24 drugs targeting either calpains or ER-stress. We demonstrated that Rho loss of function
25
26 did not activate ER-stress pathways but induced cell death through activation of calpains.
27
28 In photoreceptors bearing the P23H dominant mutation both pathways were activated but
29
30 ER stress appeared to play a critical role. Finally, we showed the protective effects in more
31
32 than one murine model by targeting both pathways with a drug combination.
33
34
35
36
37
38
39
40
41
42
43
44
45
46
47
48
49
50
51
52
53
54
55
56
57
58
59
60

Results

Activation of Calpains and Aif in dying rod cells bearing mutations in the *Rho* gene

To study the molecular effects of a dominant compared to a recessive mutation in the *Rho* gene, we evaluated cell death pathways activated in rod photoreceptors. We analyzed the transgenic mouse expressing human P23H RHO ($P23H^{Tg}$) (14), the knock-in P23H mouse (17) bred to eliminate the wild type Rho allele ($Rho^{P23H/-}$) and compared them to the homozygous Rho knock-out mouse ($Rho^{-/-}$) (26). We chose to study the P23H mutation in the absence of wild type Rho in one of the murine models to uncover molecular mechanisms activated by the mutation and limit protecting effects from the wild type protein (9). The peaks of cell death in the retinas of these chosen murine models were post-natal day 9 (PN9) for $P23H^{Tg}$, PN16 for $Rho^{P23H/-}$ and PN45 for $Rho^{-/-}$ (as reported in (27) and shown in Figure S1 A). Lack of the wild type allele in the $Rho^{P23H/-}$ retina caused a more rapid degeneration compared to the published phenotype in $Rho^{P23H/+}$ (17, 28). Previous studies reported that the P23H mutation did not cause a reduction of *Rho* mutant mRNA rather lower levels of P23H mutant Rho protein as well as unpaired glycosylation (16, 17). We thus analyzed Rho protein in mutant retinas from $Rho^{P23H/-}$ and $P23H^{Tg}$ (in the absence of the endogenous wild type allele) before and at their peaks of cell death. Here the P23H mutant Rho monomer (open arrow) appeared less abundant compared to wild type Rho at the same age (Figure S1 B), in line with reports analyzing expression of Rho in $Rho^{P23H/P23H}$ retinas and other mutant alleles expressed in the absence of wild type Rho (9, 17, 28). Retinas expressing only P23H mutant Rho had more forms at higher molecular weights that probably represent aggregates/multimers, as reported *in vitro* and *in vivo* for dominant RHO mutations (9, 29–31). Moreover, immunofluorescence analyses showed accumulation of P23H mutant Rho around the nuclei of photoreceptors suggesting that it aggregates inside the cells (Figure S1 C).

1
2
3 We previously characterized the molecular pathways of cell death in the *rd1* mouse
4 model of RP and showed that calpain and Aif play key roles in photoreceptor demise (19,
5 27). Activation of calpains was reported in several rodent models of RP and we reported
6 calpain activation in *P23H^{Tg}* and *Rho^{-/-}* degenerating retinas (32, 33). In this study we
7 confirmed activation of calpains in all the chosen mouse models by assessing the
8 cleavage of α II-spectrin, a substrate for calpains (34) as well as by using the previously
9 published *in situ* calpain activity assay (19, 20, 27). Protein analysis confirmed an increase
10 of the 145 kDa fragment of α II-spectrin consistent with cleavage by calpains (Figure 1 A,
11 arrow). Retinas expressing P23H mutant Rho also showed 120 kDa fragments possibly
12 derived from activation of caspases (asterisk). Here we *in situ* confirmed activation of
13 calpains also in *Rho^{P23H/-}* photoreceptors at PN16 (Figure S1 D). Double labeling of
14 calpain activity with TUNEL indicated that about 50% of dying cells in PN9 *P23H^{Tg}* and
15 PN16 *Rho^{P23H/-}* retinas activated calpains while calpains contributed more prominently to
16 cell death in the *Rho^{-/-}* mutant retina by labeling about 90% of TUNEL⁺ cells (Figure 1 B).

17
18
19 We then evaluated Aif activation and nuclear translocation by immunofluorescence
20 imaging and immunoblotting of nuclear extracts derived from wild type and Rho mutant
21 retinas. Aif translocation into the photoreceptor nuclei of these three murine models was
22 high at their peaks of cell death (Figure 1 C, arrows and [Figure S1 E-G](#)). We counted cells
23 with nuclear localization of Aif that were co-labeled by TUNEL and found that about 50%
24 of both *P23H^{Tg}* and *Rho^{P23H/-}* dying cells showed Aif inside their nuclei, similar to cells
25 activating calpains (Figure 1 D). A stronger correlation of Aif activation with TUNEL was
26 observed in *Rho^{-/-}* retinas (Figure 1 D). Aif translocation into the nuclei of dying
27 photoreceptor cells was confirmed by immunoblotting that compared nuclear extracts from
28 wild type and mutant retinas (Figure 1 E). Altogether these data demonstrate that calpains
29
30
31
32
33
34
35
36
37
38
39
40
41
42
43
44
45
46
47
48
49
50
51
52
53
54
55
56
57
58
59
60

1
2
3 are activated and Aif translocates into the nuclei of photoreceptor cells in mouse models of
4
5 RP caused by Rho mutations.
6

7
8 Activation of calpains can be induced by increase of intracellular calcium as reported in
9
10 the *rd1* mutant retina (19, 34). Using a fluorescent dye we compared calcium levels in wild
11
12 type and mutant photoreceptors and found more photoreceptor cells with high levels of
13
14 calcium in retinas bearing mutations in Rho (Figure S2).
15
16
17

18 **Calpains activate Aif in Rho mutant retinas**

19
20 To address whether Aif is activated by calpains in Rho mutant retinas we injected mice
21
22 intravitreally with the calpain-specific inhibitor calpastatin peptide either at PN9 (*P23H^{Tg}*) or
23
24 at PN15 (*Rho^{P23H/-}*) or at PN44 (*Rho^{-/-}*). Retinas were analyzed at PN10 for *P23H^{Tg}*, PN16
25
26 for *Rho^{P23H/-}* and PN45 for *Rho^{-/-}*, respectively. The injection protocol was similar to the
27
28 previously published method (20). Effectiveness of calpastatin peptide treatment was
29
30 confirmed by the reduction of the 145 kDa fragment of α II-spectrin (Figure 2 A, arrow). We
31
32 also observed a significant reduction of the number of photoreceptors activating calpains,
33
34 based on the *in situ* calpain activity assay (Figure 2 B). Sixteen hours after calpastatin
35
36 peptide injection, we detected a strong reduction of cell death in *Rho^{-/-}* retinas as defined
37
38 by the loss of TUNEL labeled cells as well as a decrease of cells showing activation of Aif
39
40 (Figure 2 C-E). Activated Aif protein inside the nuclei was undetectable in *Rho^{-/-}* retinas
41
42 after treatment with calpastatin peptide (Figure 2 C). Calpain inhibition was thus very
43
44 effective in reducing cell demise in retinas bearing recessive mutations in the *Rho* gene.
45
46 Calpastatin peptide, significantly but at a lower level, reduced cell death and Aif nuclear
47
48 translocation in retinas expressing the P23H mutation (Figure 2 C-E). This limited effect of
49
50 calpain inhibition implies that calpains and Aif are not the only cell death factors triggered
51
52 in photoreceptors cells expressing dominant mutations in Rho.
53
54
55
56
57
58
59
60

Activation of ER-stress in P23H Rho mutant rods

Activation of ER-stress was previously shown in rodent P23H mutant retinas (23, 35). We wished to define the timing of activation of Ire1 and Perk ER-stress sensors in our murine models expressing mutant Rho and correlate this to cell death as defined by TUNEL staining. No activation of ER stress sensors was detectable in *Rho*^{-/-} retinas at any time point during degeneration (data not shown), thus the homozygous recessive model was not further analyzed in this study. Activation of Ire1, defined by detection of phosphorylated Ire1, was observed in *P23H*^{Tg} retinas with a marked decrease at PN10 (Figure 3 A). To confirm that Ire1 phosphorylation activated the pathway, we evaluated the alternative splicing of *Xbp1* with specific primers for spliced *Xbp1* (*sXbp1*). Splicing of *Xbp1* (*sXbp1*) detectable at PN8 and PN9 but not at PN10 confirmed that activation of the Ire1 pathway declined with progression of retinal degeneration (Figure 3 B). Using antibodies for phosphorylated Ire1 we confirmed that phosphorylation of the ER-stress sensor Ire1 resided in photoreceptor cells and not in other retinal cells (Figure 3 C, arrow). Similar results were obtained by analyzing Ire1 phosphorylation and *Xbp1* splicing in *Rho*^{P23H/-} retinas (Figure 4 A-C). The Perk pathway otherwise was activated at all evaluated time points during retinal degeneration in both mutant retinas as demonstrated by phosphorylation of Perk as well as by phosphorylation of Eif2 α (Figure 3 D-E and Figure 4 D-E). We also confirmed that activation of the Perk pathway occurred in photoreceptor cells by immunofluorescence of retinal sections with the anti-phospho-Perk antibody (Figure 3 F and Figure 4 F).

Rods bearing a dominant mutation in Rho not only activate the calpain-Aif pathway but also the detrimental ER-stress pathways that together may contribute to retinal

1
2
3 degeneration. The individual impact of each of these pathways was tested by *in vivo*
4
5 treatments with specific inhibitors.
6
7
8

9 **Calpains and ER-stress contributions to cell death in P23H mutant photoreceptors**

10 To test the impact of calpains on ER-stress we treated $P23H^{Tg}$ and $Rho^{P23H/-}$ degenerating
11
12 eyes *in vivo* with the calpastatin peptide and evaluated activations of ER-stress sensors.
13
14 $P23H^{Tg}$ eyes were intravitreally injected at the age of PN9 with calpastatin peptide and
15
16 analyzed 16 hours later; $Rho^{P23H/-}$ eyes were intravitreally injected at the age of PN15 with
17
18 calpastatin peptide and analyzed 16 hours later. The calpain inhibition had no significant
19
20 effect on Ire1 activation (Figure 5 A-D and Figure S3 A-D) nor on the Perk pathway (Figure
21
22 5 E-H and Figure S3 E-H). Blocking calpains, however, significantly reduced cell death in
23
24 both murine models expressing the P23H mutation (Figure 2E and Figure 5M).
25
26
27
28

29 We then interfered *in vivo* with ER-stress by intraperitoneal injection of salubrinal, an
30
31 inhibitor of Eif2 α dephosphorylation and thus of ER-stress (36). Salubrinal protected
32
33 $P23H^{Tg}$ rod photoreceptors from cell death reducing by 74% the number of TUNEL
34
35 positive cells and by 50% $Rho^{P23H/-}$ mutant photoreceptors (Figure 5 M). Immunoblottings
36
37 confirmed that salubrinal increased Eif2 α phosphorylation in the retina without increased
38
39 activation of Perk (Figure 5 E-H and Figure S3 E-H). We observed that salubrinal
40
41 maintained higher levels of phosphorylated Ire1 and spliced *Xbp1* in PN10 $P23H^{Tg}$ retinas
42
43 and in PN16 $Rho^{P23H/-}$ retinas (Figure 5 A-D and Figure S3 A-D), ages when
44
45 phosphorylated Ire1 is reduced (see Figures 3 A-B and Figure 4 A-B). The protective effect
46
47 of salubrinal may thus be mediated by a sustained UPR. Salubrinal treatment had no
48
49 effect on calpains because it did not reduce the number of photoreceptor cells activating
50
51 calpains in $P23H^{Tg}$ and in $Rho^{P23H/-}$ retinas (Figure 5 N). After interference of ER-stress
52
53 with salubrinal, nuclear translocation of Aif was significantly affected in $P23H^{Tg}$ and in
54
55
56
57
58
59
60

1
2
3 *Rho*^{P23H/-} as defined by nuclear translocation analyses (Figure 5 I-J and Figure S3 I-J) and
4
5 by counting cells double labeled by nuclear Aif and TUNEL (Figure 5 O).
6

7 Bip/Grp79 is a member of the Hsp70 family of chaperones that regulate ER stress
8 signaling by binding to Ire1 and Perk. Over-expression of Bip/Grp79 in P23H mutant
9 retinas was previously reported to be protective and to reduce retinal degeneration (23).
10 We thus analyzed the Bip/Grp79 in retinas before and after treatments and found that
11 salubrinal, but not calpastatin, increased Bip/Grp79 protein levels (Figure 5 K-L and Figure
12 S3 K-L).
13
14
15
16
17
18
19
20
21
22

23 **Targeting Calpains and ER-stress has additive protective effects in rod** 24 **photoreceptors expressing P23H mutant Rho**

25 Data described so far could not define if the different treatments were blocking the same
26 cell death pathway at different levels or were interfering with different pathways activated
27 in parallel. To address this question we co-treated mice with salubrinal and calpastatin
28 peptide *in vivo*. The effects of salubrinal on the ER stress sensors were maintained also in
29 the presence of calpastatin peptide, as demonstrated by increase in phosphorylation of
30 Eif2 α and of Ire1 (Figure 5 A-H and Figure S3 A-H). The combined treatment with
31 salubrinal and calpastatin peptide also increased the levels of Bip/Grp79 protein in both
32 murine models expressing the P23H mutant Rho (Figure 5 K-L and Figure S3 K-L). This
33 treatment had a stronger protective effect than either drug alone. In fact, we could
34 measure a significant reduction of TUNEL⁺ cells (Figure 5 M) when compared to
35 treatments with calpastatin peptide in both *P23H^{Tg}* and *Rho*^{P23H/-} retinas. Decrease of cell
36 death with the combined treatment was significant when compared to treatment with
37 salubrinal only in *P23H^{Tg}* but not in *Rho*^{P23H/-} retinas. **Histological analyses show no**
38 **evidence of toxic effects on photoreceptors or other retinal neurons after treatments**
39
40
41
42
43
44
45
46
47
48
49
50
51
52
53
54
55
56
57
58
59
60

1
2
3 (Figure S4 A, C, D). The short time frame between injections and analyses helps
4
5 biochemical studies but does not allow assessment of phenotype rescue with an increased
6
7 number of photoreceptor cells or redistribution of the RHO protein (Figure S4).
8
9

10 11 12 **Discussion**

13
14 In this study we report a molecular characterization of cell death pathways in one model of
15
16 recessive RP caused by Rho loss of function and two models of dominant RP caused by
17
18 point mutations in Rho. The most interesting finding is a common mechanism of cell death,
19
20 the calpain-mediated pathway, associated with both recessive and dominant Rho
21
22 mutations. Interestingly, activation of calpains appears to be a general mechanism initiated
23
24 by photoreceptors during retinal degeneration since calpains have been found activated in
25
26 several animal models of RP (19, 20, 24, 25, 27, 33, 34, 37–41). The key role of calpains
27
28 in retinal degeneration was also demonstrated after light damage on a canine model of RP
29
30 bearing a mutation in the *RHO* gene (42). We also show co-activation of calpains and Aif
31
32 suggesting that calpains may activate Aif in response to mutations of Rho similar to what
33
34 we previously reported in the *rd1* mutant retinas (19). The reduction of Aif activation in
35
36 retinas treated with calpastatin peptide, a calpain inhibitor, confirms this hypothesis.
37
38 Calpastatin peptide is able to completely abolish Aif nuclear translocation as well as cell
39
40 death in the *Rho*^{-/-} retina but not in retinas expressing the P23H dominant mutation. This
41
42 indicates that the main cell death pathway activated in RP linked to recessive mutation in
43
44 *Rho* is mediated by calpains. We cannot exclude involvement of other mechanisms of cell
45
46 death but prolonged exposure to calpain inhibitors will be required to uncover other
47
48 players.
49
50
51
52

53
54 Activation of Aif appears to be mediated by calpains in all mutant retinas studied here,
55
56 however expression of the dominant mutation may trigger other mechanisms that affect
57
58
59
60

1
2
3 activation of Aif. In fact, in both animal models bearing the P23H mutation salubrinal
4
5 treatment caused a significant reduction of activated Aif in the retina but not of activated
6
7 calpains. The different effect on Aif and on calpains can be explained by the fact that Aif
8
9 can be activated by several proteases and among those caspases (43, 44). Activation of
10
11 caspases in retinas with dominant mutations in Rho have been previously reported (23, 24,
12
13 33, 42, 45–47) and is also suggested by our analyses of cleavage of the cytoskeletal
14
15 protein α II-spectrin that revealed lower molecular weight fragments in P23H mutant retinas,
16
17 not observed in the retina with Rho loss of function.
18
19

20
21 The expression of a dominant mutation in Rho activates additional pathways involving
22
23 ER-stress. Mutations in integral membrane proteins affecting folding cause ER retention
24
25 and are linked to diseases, as also shown for Rho (48, 49). Correlation of the ER-stress
26
27 Perk pathway with intracellular Ca^{2+} variations and with calpains was previously described
28
29 in retina and brain neurons but not well characterized (50–54). By treatment with drugs
30
31 targeting either calpains or ER-stress, we determined that these are parallel pathways. In
32
33 fact, treatment with calpastatin did not significantly affect phosphorylation of ER-stress
34
35 sensors. Similarly, treatment with salubrinal did not reduce the number of cells activating
36
37 calpains but **nearly increased calpain activity even in the presence of calpastatin.**

38
39
40 **Salubrinal was reported to only moderately reduce calpain activity when a cancer cell line**
41
42 **was pretreated with salubrinal before activation of calpains and to increase cytosolic Ca^{2+}**
43
44 **in EBV-transformed B cells (55, 56). If indeed salubrinal increases cytosolic Ca^{2+} in**
45
46 **photoreceptors as well, this may activate several calpains and not only calpain 1 and 2.**

47
48 **Calpastatin specifically blocks calpain 1 and 2 that we previously demonstrated to be**
49
50 **linked to photoreceptor cell death (27). Interfering with the two pathways in co-treatment**
51
52 **experiments showed a significant benefit when compared to single treatments confirming**
53
54 **that calpains and ER-stress are independently activated. Our study thus highlights the**
55
56
57
58
59
60

1
2
3 importance of combined treatments of dominant RP caused by mutations in the *RHO* gene.
4
5 Neuroprotective effects with salubrinal are consistent with the beneficial effects observed
6
7 in photoreceptors from a patient bearing a dominant RHO mutation (E181K) (57).
8

9
10 Interestingly, in our studies salubrinal not only increased phosphorylated Eif2 α but also
11
12 maintained activation of Ire1. Sustained expression of activated Ire1 was previously shown
13
14 to have protective effects in *Drosophila* on photoreceptors expressing mutant Rho (58).
15

16 Salubrinal was also previously reported to protect cells from the deleterious effect of ER-
17
18 stress in a *Drosophila* model of retinal degeneration (59).
19

20
21 Activation of ER-stress is consistent with the observation of high molecular weight Rho
22
23 protein in retinal extracts from mice expressing the dominant mutation. We also observed
24
25 a different distribution of the protein in the photoreceptor cells. These data are partially
26
27 discordant with a study of the knock-in mouse expressing two P23H mutant alleles (28).
28
29 The apparent discrepancy may be due to the different genotypes of the mice used in the
30
31 two studies. In fact, in this study we analyzed mice bearing a single mutant allele in the
32
33 absence of the wild type allele while the published study analyzed mice with two P23H
34
35 mutant alleles. A second explanation may reside with the methods used here for epitope
36
37 retrieval in immunofluorescence experiments and for protein extraction in immunoblotting.
38
39 In fact, different detergents were reported to affect the Rho pattern during immunoblotting
40
41 (60).
42
43
44

45 Recessive mutations are rare in the *RHO* gene and the only confirmed null mutation is
46
47 the E249X mutation identified in one patient (4). The loss of function effects of the second
48
49 mutation, E150K, found in homozygosity in patients is still controversial because molecular
50
51 and functional studies in the recently generated knock-in mouse identify this mutation as a
52
53 slowly progressing adRP (61).
54
55
56
57
58
59
60

1
2
3 In summary, our study demonstrates that dominant and recessive mutations in the *Rho*
4 gene trigger different responses in photoreceptor cells. While clinical symptoms are similar
5 in patients with adRP and arRP, RP caused by the P23H mutation is not due to
6 haploinsufficiency, and therapeutic strategies will need to account for the different
7 molecular events triggered by different mutations. Our study only assessed the effects of
8 calpastatin peptide and salubrinal on the retina after 16 hours of exposure analyzing the
9 number of TUNEL⁺ cells and activation of the pathways, these experiments are therefore
10 not appropriate to evaluate preservation of the number and morphology of rod and cone
11 photoreceptors. Long-term effects of these drugs in the eye as well as neuroprotective
12 activities need to be evaluated for their therapeutic use in retinal degeneration. Treatments
13 *in vivo* with salubrinal or continuous expression of calpastatin in the forebrain of transgenic
14 mice did not show adverse effects, but long-term exposure in the eye was not assessed
15 (62–66). The identification of the two cell death pathways paves the way for specific
16 pharmacological screenings to identify new, safe and effective drugs for the treatment of
17 this blinding disease.
18
19
20
21
22
23
24
25
26
27
28
29
30
31
32
33
34
35
36
37
38
39
40
41
42
43
44
45
46
47
48
49
50
51
52
53
54
55
56
57
58
59
60

Materials and Methods

Animal care

All procedures on mice were conducted at CSSI (Centro Servizi Stabulario Interdipartimentale) and approved by the Ethical Committee of University of Modena and Reggio Emilia (Prot. N. 106 22/11/2012) and by the Italian Ministero della Salute (346/2015-PR). Rhodopsin P23H transgenic mice ($P23H^{Tg}$) (14) were kindly provided by M. Humphries and T. Dryja and bred on a C57BL/6J genetic background, C57BL/6J wild-type mice were purchased from Envigo Italy (Udine, IT). We chose to maintain the endogenous murine Rho in this model because, in the absence of endogenous Rho, retinal degeneration proceeds rapidly affecting our analyses. $Rho^{-/-}$ mice in a 129/sv background (26) were kindly provided by M. Humphries. The P23H knock-in mice in a C57BL/6J background (17) were mated with the Rho knock-out mice to obtain mice with one Rho null allele and one P23H mutant Rho allele ($Rho^{P23H/-}$). Mice were maintained in a 12hr light/dark cycle and had free access to food and water.

In vivo treatments

For intravitreal administration, mice at the age of 9 days after birth (PN9) or PN15 or PN44 were anesthetized with an intraperitoneal injection of 250 mg/kg body weight of avertin (1.25% (w/v) 2,2,2-tribromoethanol and 2.5% (v/v) 2-methyl-2-butanol; Sigma, Milan, IT). Subsequently, the eyelid was opened and a 34GA needle was inserted adjacent to the limbal border of the cornea. 0.5 μ l of calpastatin peptide (200 μ M solution, with an expected final concentration in the eye of 20 μ M; Calbiochem, Milan, IT) were delivered intravitreously and the control eyes received vehicle only (PBS). Salubrinal was injected twice per day intraperitoneally starting at the age of PN7 (50 μ l of a 1:50 dilution in 0.9%

1
2
3 NaCl of a 5 mg/ml stock solution in DMSO; Calbiochem). Control mice received the same
4
5 volume of vehicle (2% DMSO in 0.9% NaCl).
6
7
8

9 10 **Calpain activity assay**

11 Cryosections from unfixed retinas were incubated for 15 min in calpain reaction buffer
12 (CRB: 25 mM HEPES-KOH pH 7.2, 65 mM KCl, 2 mM MgCl₂, 1.5 mM CaCl₂, 2 mM DTT)
13 and then exposed for 1 h at 37°C to the fluorescent calpain substrate CMAC, t-BOC-Leu-
14 Met (A6520, Life Technologies, Monza, IT) at a final concentration of 2 µM as in (20).
15
16 Slides were analyzed at an Axioskop 40 fluorescence microscope (Zeiss, Arese, IT) using
17 the filter excitation/emission wavelengths of 365/420 nm.
18
19
20
21
22
23
24
25
26

27 **DNA Nick-End Labeling by TUNEL and immunofluorescence**

28 Eyes were oriented, fixed in Davidson's fixative (8% Formaldehyde, 31.5% Ethanol, 2 M
29 Acetic Acid), embedded in paraffin and 5 µm sections along the superior-inferior axis were
30 collected. Apoptotic nuclei were detected by TdT-mediated dUTP terminal nick-end
31 labeling kit (TUNEL, fluorescein; Roche, Milan, IT) used according to the manufacturer's
32 protocols. Sections were boiled with 10 mM Tris-HCl pH 9, incubated at 60°C for 10 min
33 and at room temperature for 30 min. Primary antibodies were employed as follows: anti-Aif
34 (1:100; Sigma), anti-Perk (1:50, H-300: sc-13073, Santa Cruz Biotechnology), anti-
35 phosphorylated Ire1 (1:100, Novus Biologicals, Milan, IT), anti-phosphorylated Perk (1:100,
36 Cell Signaling), anti-Rho (1:1000, 1D4; Sigma). Secondary antibodies were Oregon
37 Green® 488 anti-mouse, Alexa Fluor® 568 anti-mouse, anti-goat and anti-rabbit antibodies
38 (Life Technologies). Slides were mounted with mowiol 4-88 (Sigma) and analyzed with an
39
40
41
42
43
44
45
46
47
48
49
50
51
52
53
54
55
56
57
58
59
60

1
2
3 performed by counting all labeled cells in the photoreceptor cell layer passing through the
4
5 optic nerve in at least 3 sections from different animals.
6
7

8 9 10 **Cytofluorimetric analysis of calcium**

11 Intracellular calcium levels were determined with the intracellular calcium probe Fluo-4 AM
12 (Life Technologies). Retinas were incubated in 19 U/ml papain for 30 min and, after 33-fold
13 dilution with DMEM containing 10 U/ml DNase, retina cells were dissociated by trituration.
14 After three washes with PBS, cells were incubated with Fluo-4 AM at 37°C for 30 min in
15 Ca^{2+} -free medium. Fluorescence was measured with a Coulter Epics XL-MCL flow
16 cytometer (Beckman Coulter) at an excitation wavelength of 488nm. Photoreceptor cells
17 stained with anti-Rho antibody 1D4 (1:1000, Sigma) had been previously characterized as
18 in (67) and plotted over the forward scatter to define the gating strategy for the following
19 intracellular calcium analysis (see Figure S2 A). Fluo4 AM signal was measured at PN10
20 for P23H^{Tg}, PN16 for Rho^{P23H/-} and PN45 for Rho^{-/-} in at least three different retinas and
21 the percentages of cells with high fluorescence were compared to the age-matched wild
22 type controls.
23
24
25
26
27
28
29
30
31
32
33
34
35
36
37
38
39
40

41 **RT-PCR**

42 Total RNA was extracted from murine retinas with Trizol (Life Technologies) and cDNA
43 was synthesized using the Transcriptor High Fidelity cDNA Synthesis Kit (Roche). PCR
44 analysis of the spliced form of *Xbp1* was performed with primers specifically recognizing
45 the spliced variant (sXbp1-f: GGTCTGCTGAGTCCGCAGCAGG and sXbp1-r:
46 CAGGCCTATGCTATCCTCTAGGC) with the following protocol: 10 min at 95°C followed
47 by 30 cycles composed by 30 sec at 95°C, 30 sec at 64°C and 90 sec at 72°C. The
48
49
50
51
52
53
54
55
56
57
58
59
60

1
2
3 expected PCR product consisted of 718 bp. PCR was normalized with primers for the S26
4 gene (S26-f: AAGTTTGTCATTCGGAACATT and S26-r: GATCGATTCTAACAACCTTG).
5
6
7
8

9 **Retinal protein extracts and Western blotting analysis**

10 Retinas were dissected in PBS. Total cell extracts were prepared by homogenizing retinas
11 in 20 mM Tris-HCl pH 7.4, 150 mM NaCl, 1% CHAPS, 0.2 mM Na₃PO₄, 1 mM Na₃VO₄,
12 protease inhibitor cocktail (Sigma) and centrifugation at 17000xg for 10 min. For nuclei-
13 enriched lysate preparation, retinas were transferred into a 2 ml Dounce homogenizer with
14 200 µl of cold homogenizing buffer (20 mM HEPES-KOH pH 7.5, 250 mM sucrose, 10 mM
15 KCl, 1.5 mM MgCl₂, 2 mM EDTA, 1 mM DTT, 0.2 mM Na₃PO₄, 1 mM Na₃VO₄, protease
16 inhibitor cocktail from Sigma) and placed on ice for 30 min. The tissue was disrupted with
17 40 strokes and centrifuged at 900xg for 5 min at 4°C to isolate the nuclear fraction. The
18 pellet was washed twice in cold homogenizing buffer and resuspended in lysis buffer (50
19 mM Tris-HCl pH 7.4, 150 mM NaCl, 1% NP-40, 0.1% SDS, 1 mM EDTA, 0.2 mM Na₃PO₄,
20 1 mM Na₃VO₄, protease inhibitor cocktail from Sigma). The purity of enriched lysates was
21 checked by western blotting with a nuclear marker (anti-Histone H3 1:3000; Bethyl
22 Laboratories, Bologna, IT) and a cytosol marker (anti-pan-actin, 1:3000, Millipore).
23
24
25
26
27
28
29
30
31
32
33
34
35
36
37
38
39

40 Equivalent amounts of protein extracts (3 µg for total extracts, 20 µg for nuclear extracts
41 and 80 µg for analyses of αII-spectrin) were resolved using SDS-PAGE and
42 immunoblottings were performed following standard procedures. The antibodies used for
43 immunoblotting were: anti-Aif (1:1000; Oncogene), anti-αII-spectrin (anti-fodrin; 1:2000,
44 Enzo Life, Roma, IT), anti-Bip (1:1000, Santa Cruz Biotechnology), anti-Eif2α (1:1000, Cell
45 Signaling), anti-Histone H3 (1:3000; Bethyl Laboratories), anti-phosphorylated-Ire1
46 (1:2000, Novus Biologicals), anti-phosphorylated-Perk (1:1000, Cell Signaling), anti-
47 phosphorylated-Eif2α (1:1000, Cell Signaling), anti-Perk (1:1000, Santa Cruz
48
49
50
51
52
53
54
55
56
57
58
59
60

1
2
3 Biotechnology), anti-pan-actin (1:3000, Millipore), and anti-recoverin (1:1000, Millipore).
4
5 Quantification was performed by densitometry analysis of scanned images with ImageJ
6
7 software, corrected for background and plotted as protein/normalizing protein. Data are
8
9 presented as means \pm SD of 3 blots with proteins derived as biological replicates from 3
10
11 animals.
12

13 14 15 16 **Statistical analysis**

17
18 Cell counts and densitometry analyses are shown as means \pm SD. Paired Student's t-test
19
20 analysis was performed to compare data derived from at least three different wild-type or
21
22 mock treated mutant retinas to at least three different mutant or drug treated retinas,
23
24 respectively.
25
26
27
28
29
30
31
32
33
34
35
36
37
38
39
40
41
42
43
44
45
46
47
48
49
50
51
52
53
54
55
56
57
58
59
60

Acknowledgments

Authors would like to thank Alessandra Recchia and Francesca Fanelli for helpful discussion. We acknowledge the CIGS (Cinzia Restani) and CSSI of University of Modena and Reggio Emilia for providing confocal microscopy and animal husbandry assistance as well as the Cell-lab facility at University of Modena and Reggio Emilia. K.P. is the John H. Hord Professor of Pharmacology. This work was supported by research grant GGP11201A from Fondazione Telethon, E-RARE 2009 RHORCOD; by Programma di ricerca Regione-Università 2010-2012 of Regione Emilia Romagna (RARER); by research grant of Fondazione Roma (call for proposal 2013 sulla Retinite Pigmentosa); The Arnold and Mabel Beckman Foundation; and Foundation Fighting Blindness.

Conflict of interest disclosure

None.

References

1. Hartong, D.T., Berson, E.L. and Dryja, T.P. (2006) Retinitis pigmentosa. *Lancet*, **368**, 1795–1809.
2. Trifunović, D., Karali, M., Camposampiero, D., Ponzin, D., Banfi, S. and Marigo, V. (2008) A high-resolution RNA expression atlas of retinitis pigmentosa genes in human and mouse retinas. *Invest Ophthalmol Vis Sci*, **49**, 2330–2336.
3. Kumaramanickavel, G., Maw, M., Denton, M.J., John, S., Srikumari, C.R., Orth, U., Oehlmann, R. and Gal, A. (1994) Missense rhodopsin mutation in a family with recessive RP. *Nat Genet*, **8**, 10–11.
4. Rosenfeld, P.J., Cowley, G.S., McGee, T.L., Sandberg, M.A., Berson, E.L. and Dryja, T.P. (1992) A null mutation in the rhodopsin gene causes rod photoreceptor dysfunction and autosomal recessive retinitis pigmentosa. *Nat Genet*, **1**, 209–213.
5. Filipek, S., Stenkamp, R.E., Teller, D.C. and Palczewski, K. (2003) G protein-coupled receptor rhodopsin: a prospectus. *Annu Rev Physiol*, **65**, 851–879.
6. Hargrave, P.A. (2001) Rhodopsin structure, function, and topography the Friedenwald lecture. *Invest Ophthalmol Vis Sci*, **42**, 3–9.
7. Palczewski, K. (2006) G protein-coupled receptor rhodopsin. *Ann Rev Biochem*, **75**, 743–767.
8. Lin, J.H., Li, H., Yasumura, D., Cohen, H.R., Zhang, C., Panning, B., Shokat, K.M., LaVail, M.M. and Walter, P. (2007) IRE1 signaling affects cell fate during the unfolded protein response. *Science (80-)*, **318**, 944–949.
9. Frederick, J.M., Krasnoperova, N. V, Hoffmann, K., Church-Kopish, J., Ruther, K., Howes, K., Lem, J. and Baehr, W. (2001) Mutant rhodopsin transgene expression on a null background. *Invest Ophthalmol Vis Sci*, **42**, 826–833.
10. Griciuc, A., Aron, L. and Ueffing, M. (2011) ER stress in retinal degeneration: a target for rational therapy? *Trends Mol Med*, **17**, 442–451.
11. Griciuc, A., Aron, L., Piccoli, G. and Ueffing, M. (2010) Clearance of Rhodopsin(P23H) aggregates requires the ERAD effector VCP. *Biochim Biophys Acta*, **1803**, 424–434.
12. Dryja, T.P., McGee, T.L., Hahn, L.B., Cowley, G.S., Olsson, J.E., Reichel, E., Sandberg, M.A. and Berson, E.L. (1990) Mutations within the rhodopsin gene in patients with autosomal dominant retinitis pigmentosa. *N Engl J Med*, **323**, 1302–1307.
13. Saliba, R.S., Munro, P.M.G., Luthert, P.J. and Cheetham, M.E. (2002) The cellular fate of mutant rhodopsin: quality control, degradation and aggresome formation. *J Cell Sci*, **115**, 2907–2918.
14. Olsson, J.E., Gordon, J.W., Pawlyk, B.S., Roof, D., Hayes, A., Molday, R.S., Mukai, S., Cowley, G.S., Berson, E.L. and Dryja, T.P. (1992) Transgenic mice with a rhodopsin mutation (Pro23His): a mouse model of autosomal dominant retinitis pigmentosa. *Neuron*, **9**, 815–830.
15. Machida, S., Kondo, M., Jamison, J.A., Khan, N.W., Kononen, L.T., Sugawara, T., Bush, R.A. and Sieving, P.A. (2000) P23H rhodopsin transgenic rat: correlation of retinal function with histopathology. *Invest Ophthalmol Vis Sci*, **41**, 3200–3209.
16. Price, B.A., Sandoval, I.M., Chan, F., Simons, D.L., Wu, S.M., Wensel, T.G. and Wilson, J.H. (2011) Mislocalization and Degradation of Human P23H-Rhodopsin-GFP

- 1
2
3 in a Knockin Mouse Model of Retinitis Pigmentosa. *Invest Ophthalmol Vis Sci*, **52**,
4 9728–9736.
- 5
6 17. Sakami,S., Maeda,T., Bereta,G., Okano,K., Golczak,M., Sumaroka,A., Roman,A.J.,
7 Cideciyan,A. V, Jacobson,S.G. and Palczewski,K. (2011) Probing mechanisms of
8 photoreceptor degeneration in a new mouse model of the common form of autosomal
9 dominant retinitis pigmentosa due to P23H opsin mutations. *J Biol Chem*, **286**,
10 10551–10567.
- 11
12 18. Wang,M. and Kaufman,R.J. (2016) Protein misfolding in the endoplasmic reticulum as
13 a conduit to human disease. *Nature*, **529**, 326–335.
- 14
15 19. Sanges,D., Comitato,A., Tammara,R. and Marigo,V. (2006) Apoptosis in retinal
16 degeneration involves cross-talk between apoptosis-inducing factor (AIF) and
17 caspase-12 and is blocked by calpain inhibitors. *Proc Natl Acad Sci USA*, **103**,
18 17366–17371.
- 19
20 20. Paquet-Durand,F., Sanges,D., McCall,J., Silva,J., van Veen,T., Marigo,V. and
21 Ekström,P. (2010) Photoreceptor rescue and toxicity induced by different calpain
22 inhibitors. *J Neurochem*, **115**, 930–940.
- 23
24 21. Cande,C., Vahsen,N., Kouranti,I., Schmitt,E., Daugas,E., Spahr,C., Luban,J.,
25 Kroemer,R.T., Giordanetto,F., Garrido,C., *et al.* (2004) AIF and cyclophilin A
26 cooperate in apoptosis-associated chromatinolysis. *Oncogene*, **23**, 1514–1521.
- 27
28 22. Moubarak,R.S., Yuste,V.J., Greer,P.A., Artus,C., Bouharrou,A., Menissier-de Murcia,J.
29 and Susin,S.A. (2007) Sequential activation of poly(ADP-ribose) polymerase 1,
30 calpains, and Bax is essential in apoptosis-inducing factor-mediated programmed
31 necrosis. *Mol Cell Biol*, **27**, 4844–4862.
- 32
33 23. Gorbatyuk,M.S., Knox,T., LaVail,M.M., Gorbatyuk,O.S., Noorwez,S.M.,
34 Hauswirth,W.W., Lin,J.H., Muzyczka,N. and Lewin,A.S. (2010) Restoration of visual
35 function in P23H rhodopsin transgenic rats by gene delivery of BiP/Grp78. *Proc Natl
36 Acad Sci USA*, **107**, 5961–5966.
- 37
38 24. Sizova,O.S., Shinde,V.M., Lenox,A. and Gorbatyuk,M.S. (2014) Modulation of cellular
39 signaling pathways in P23H rhodopsin photoreceptors. *Cell Signal*, **26**, 665–672.
- 40
41 25. Ozaki,T., Ishiguro,S., Hirano,S., Baba,A., Yamashita,T., Tomita,H. and Nakazawa,M.
42 (2013) Inhibitory peptide of mitochondrial μ -calpain protects against photoreceptor
43 degeneration in rhodopsin transgenic S334ter and P23H rats. *PLoS One*, **8**, e71650.
- 44
45 26. Humphries,M.M., Rancourt,D., Farrar,G.J., Kenna,P., Hazel,M., Bush,R.A.,
46 Sieving,P.A., Sheils,D.M., McNally,N., Creighton,P., *et al.* (1997) Retinopathy induced
47 in mice by targeted disruption of the rhodopsin gene. *Nat Genet*, **15**, 216–219.
- 48
49 27. Comitato,A., Sanges,D., Rossi,A., Humphries,M.M. and Marigo,V. (2014) Activation of
50 Bax in Three Models of Retinitis Pigmentosa. *Invest Ophthalmol Vis Sci*, **55**, 3555–
51 3562.
- 52
53 28. Chiang,W.-C., Kroeger,H., Sakami,S., Messah,C., Yasumura,D., Matthes,M.T.,
54 Coppinger,J.A., Palczewski,K., LaVail,M.M. and Lin,J.H. (2015) Robust Endoplasmic
55 Reticulum-Associated Degradation of Rhodopsin Precedes Retinal Degeneration. *Mol
56 Neurobiol*, **52**, 679–695.
- 57
58 29. Colley,N.J., Cassill,J.A., Baker,E.K. and Zuker,C.S. (1995) Defective intracellular
59 transport is the molecular basis of rhodopsin-dependent dominant retinal
60 degeneration. *Proc Natl Acad Sci USA*, **92**, 3070–3074.

- 1
2
3 30. Mendes,H.F. and Cheetham,M.E. (2008) Pharmacological manipulation of gain-of-
4 function and dominant-negative mechanisms in rhodopsin retinitis pigmentosa. *Hum*
5 *Mol Genet*, **17**, 3043–3054.
6
7 31. Parfitt,D.A., Aguila,M., McCulley,C.H., Bevilacqua,D., Mendes,H.F., Athanasiou,D.,
8 Novoselov,S.S., Kanuga,N., Munro,P.M., Coffey,P.J., *et al.* (2014) The heat-shock
9 response co-inducer arimoclomol protects against retinal degeneration in rhodopsin
10 retinitis pigmentosa. *Cell Death Dis*, **5**, e1236.
11
12 32. Arango-Gonzalez,B., Trifunović,D., Sahaboglu,A., Kranz,K., Michalakis,S., Farinelli,P.,
13 Koch,S., Koch,F., Cottet,S., Janssen-Bienhold,U., *et al.* (2014) Identification of a
14 common non-apoptotic cell death mechanism in hereditary retinal degeneration. *PLoS*
15 *One*, **9**, e112142.
16
17 33. Kaur,J., Menci,S., Sahaboglu,A., Farinelli,P., van Veen,T., Zrenner,E., Ekström,P.A.,
18 Paquet-Durand,F. and Arango-Gonzalez,B. (2011) Calpain and PARP activation
19 during photoreceptor cell death in P23H and S334ter rhodopsin mutant rats. *PLoS*
20 *One*, **6**, e22181.
21
22 34. Doonan,F., Donovan,M. and Cotter,T.G. (2005) Activation of Multiple Pathways during
23 Photoreceptor Apoptosis in the rd Mouse. *Invest Ophthalmol Vis Sci*, **46**, 3530–3538.
24
25 35. Kroeger,H., Messah,C., Ahern,K., Gee,J., Joseph,V., Matthes,M.T., Yasumura,D.,
26 Gorbatyuk,M.S., Chiang,W.-C., LaVail,M.M., *et al.* (2012) Induction of Endoplasmic
27 Reticulum Stress Genes, BiP and Chop, in Genetic and Environmental Models of
28 Retinal Degeneration. *Invest Ophthalmol Vis Sci*, **53**, 7590–7599.
29
30 36. Boyce,M., Bryant,K.F., Jousse,C., Long,K., Harding,H.P., Scheuner,D., Kaufman,R.J.,
31 Ma,D., Coen,D.M., Ron,D., *et al.* (2005) A selective inhibitor of eIF2alpha
32 dephosphorylation protects cells from ER stress. *Science (80-)*, **307**, 935–939.
33
34 37. Sancho-Pelluz,J., Arango-Gonzalez,B., Kustermann,S., Romero,F.J., van Veen,T.,
35 Zrenner,E., Ekström,P. and Paquet-Durand,F. (2008) Photoreceptor cell death
36 mechanisms in inherited retinal degeneration. *Mol Neurobiol*, **38**, 253–269.
37
38 38. Paquet-Durand,F., Azadi,S., Hauck,S.M., Ueffing,M., van Veen,T. and Ekström,P.
39 (2006) Calpain is activated in degenerating photoreceptors in the rd1 mouse. *J*
40 *Neurochem*, **96**, 802–814.
41
42 39. Trifunović,D., Dengler,K., Michalakis,S., Zrenner,E., Wissinger,B. and Paquet-
43 Durand,F. (2010) cGMP-dependent cone photoreceptor degeneration in the cpfl1
44 mouse retina. *J Comp Neurol*, **518**, 3604–3617.
45
46 40. Sothilingam,V., Garcia Garrido,M., Jiao,K., Buena-Atienza,E., Sahaboglu,A.,
47 Trifunović,D., Balendran,S., Koepfli,T., Mühlfriedel,R., Schön,C., *et al.* (2015) Retinitis
48 pigmentosa: impact of different Pde6a point mutations on the disease phenotype.
49 *Hum Mol Genet*, **24**, 5486–5499.
50
51 41. Marigo,V. (2007) Programmed Cell Death in Retinal Degeneration. *Cell Cycle*, **6**, 652–
52 655.
53
54 42. Marsili,S., Genini,S., Sudharsan,R., Gingrich,J., Aguirre,G.D. and Beltran,W.A. (2015)
55 Exclusion of the unfolded protein response in light-induced retinal degeneration in the
56 canine T4R RHO model of autosomal dominant retinitis pigmentosa. *PLoS One*, **10**,
57 e0115723.
58
59 43. Lakhani,S.A., Masud,A., Kuida,K., Porter Jr.,G.A., Booth,C.J., Mehal,W.Z., Inayat,I.
60 and Flavell,R.A. (2006) Caspases 3 and 7: key mediators of mitochondrial events of

- 1
2
3 apoptosis. *Science* (80-), **311**, 847–851.
- 4
5 44. Arnoult,D., Gaume,B., Karbowski,M., Sharpe,J.C., Cecconi,F. and Youle,R.J. (2003)
6 Mitochondrial release of AIF and EndoG requires caspase activation downstream of
7 Bax/Bak-mediated permeabilization. *Embo J*, **22**, 4385–4399.
- 8
9 45. Samardzija,M., Wenzel,A., Thiersch,M., Frigg,R., Remé,C. and Grimm,C. (2006)
10 Caspase-1 Ablation Protects Photoreceptors in a Model of Autosomal Dominant
11 Retinitis Pigmentosa. *Invest Ophthalmol Vis Sci*, **47**, 5181–5190.
- 12
13 46. Liu,C., Li,Y., Peng,M., Laties,A.M. and Wen,R. (1999) Activation of caspase-3 in the
14 retina of transgenic rats with the rhodopsin mutation s334ter during photoreceptor
15 degeneration. *J Neurosci*, **19**, 4778–4785.
- 16
17 47. Zeiss,C.J., Neal,J. and Johnson,E.A. (2004) Caspase-3 in postnatal retinal
18 development and degeneration. *Invest Ophthalmol Vis Sci*, **45**, 964–970.
- 19
20 48. Castro-Fernández,C., Maya-Núñez,G. and Conn,P.M. (2005) Beyond the signal
21 sequence: protein routing in health and disease. *Endocr Rev*, **26**, 479–503.
- 22
23 49. Mendes,H.F., van der Spuy,J., Chapple,J.P. and Cheetham,M.E. (2005) Mechanisms
24 of cell death in rhodopsin retinitis pigmentosa: implications for therapy. *Trends Mol
25 Med*, **11**, 177–185.
- 26
27 50. Badiola,N., Penas,C., Miñano-Molina,A., Barneda-Zahonero,B., Fadó,R., Sánchez-
28 Opazo,G., Comella,J.X., Sabriá,J., Zhu,C., Blomgren,K., *et al.* (2011) Induction of ER
29 stress in response to oxygen-glucose deprivation of cortical cultures involves the
30 activation of the PERK and IRE-1 pathways and of caspase-12. *Cell Death Dis*, **2**,
31 e149.
- 32
33 51. Han,G., Casson,R.J., Chidlow,G. and Wood,J.P.M. (2014) The Mitochondrial Complex
34 I Inhibitor Rotenone Induces Endoplasmic Reticulum Stress and Activation of GSK-3 β
35 in Cultured Rat Retinal Cells. *Invest Ophthalmol Vis Sci*, **55**, 5616–5628.
- 36
37 52. Janyou,A., Changtam,C., Suksamrarn,A., Tocharus,C. and Tocharus,J. (2015)
38 Suppression effects of O-demethyl-demethoxycurcumin on thapsigargin triggered on
39 endoplasmic reticulum stress in SK-N-SH cells. *Neurotoxicology*, **50**, 92–100.
- 40
41 53. Lu,T.-H., Su,C.-C., Tang,F.-C., Chen,C.-H., Yen,C.-C., Fang,K.-M., Lee,K.-I., Hung,D.-
42 Z. and Chen,Y.-W. (2015) Chloroacetic acid triggers apoptosis in neuronal cells via a
43 reactive oxygen species-induced endoplasmic reticulum stress signaling pathway.
44 *Chem Biol Interact*, **225**, 1–12.
- 45
46 54. de la Cadena,S.G., Hernández-Fonseca,K., Camacho-Arroyo,I. and Massieu,L. (2014)
47 Glucose deprivation induces reticulum stress by the PERK pathway and caspase-7-
48 and calpain-mediated caspase-12 activation. *Apoptosis*, **19**, 414–427.
- 49
50 55. Park,G. Bin, Kim,Y.S., Lee,H.-K., Song,H., Kim,S., Cho,D.-H. and Hur,D.Y. (2011)
51 Reactive oxygen species and p38 MAPK regulate Bax translocation and calcium
52 redistribution in salubrinal-induced apoptosis of EBV-transformed B cells. *Cancer Lett*,
53 **313**, 235–248.
- 54
55 56. Yang,W., Tiffany-Castiglioni,E., Koh,H.C. and Son,I.-H. (2009) Paraquat activates the
56 IRE1/ASK1/JNK cascade associated with apoptosis in human neuroblastoma SH-
57 SY5Y cells. *Toxicol Lett*, **191**, 203–210.
- 58
59 57. Yoshida,T., Ozawa,Y., Suzuki,K., Yuki,K., Ohyama,M., Akamatsu,W., Matsuzaki,Y.,
60 Shimmura,S., Mitani,K., Tsubota,K., *et al.* (2014) The use of induced pluripotent stem
cells to reveal pathogenic gene mutations and explore treatments for retinitis

- 1
2
3 pigmentosa. *Mol Brain*, **7**, 45.
- 4
5 58. Griciuc,A., Aron,L., Roux,M.J., Klein,R., Giangrande,A. and Ueffing,M. (2010)
6 Inactivation of VCP/ ter94 Suppresses Retinal Pathology Caused by Misfolded
7 Rhodopsin in *Drosophila*. *PLoS Genet*, **6**, e1001075.
- 8
9 59. Mendes,C.S., Levet,C., Chatelain,G., Dourlen,P., Fouillet,A., Dichtel-Danjoy,M.-L.,
10 Gambis,A., Ryoo,H.D., Steller,H. and Mollereau,B. (2009) ER stress protects from
11 retinal degeneration. *Embo J*, **28**, 1296–1307.
- 12
13 60. Jastrzebska,B., Maeda,T., Zhu,L., Fotiadis,D., Filipek,S., Engel,A., Stenkamp,R.E. and
14 Palczewski,K. (2004) Functional characterization of rhodopsin monomers and dimers
15 in detergents. *J Biol Chem*, **279**, 54663–54675.
- 16
17 61. Zhang,N., Kolesnikov,A. V, Jastrzebska,B., Mustafi,D., Sawada,O., Maeda,T.,
18 Genoud,C., Engel,A., Kefalov,V.J. and Palczewski,K. (2013) Autosomal recessive
19 retinitis pigmentosa E150K opsin mice exhibit photoreceptor disorganization. *J Clin
20 Invest*, **123**, 121–137.
- 21
22 62. Hamamura,K., Nishimura,A., Iino,T., Takigawa,S., Sudo,A. and Yokota,H. (2015)
23 Chondroprotective effects of Salubrinal in a mouse model of osteoarthritis. *Bone Jt.
24 Res*, **4**, 84–92.
- 25
26 63. Huang,X., Chen,Y., Zhang,H., Ma,Q., Zhang,Y. and Xu,H. (2012) Salubrinal
27 attenuates β -amyloid-induced neuronal death and microglial activation by inhibition of
28 the NF- κ B pathway. *Neurobiol Aging*, **33**, 1007.e9–1007.e17.
- 29
30 64. Higuchi,M., Tomioka,M., Takano,J., Shirotani,K., Iwata,N., Masumoto,H., Maki,M.,
31 Itohara,S. and Saido,T.C. (2005) Distinct mechanistic roles of calpain and caspase
32 activation in neurodegeneration as revealed in mice overexpressing their specific
33 inhibitors. *J Biol Chem*, **280**, 15229–15237.
- 34
35 65. Rubovitch,V., Barak,S., Rachmany,L., Goldstein,R.B., Zilberstein,Y. and Pick,C.G.
36 (2015) The neuroprotective effect of salubrinal in a mouse model of traumatic brain
37 injury. *Neuromol Med*, **17**, 58–70.
- 38
39 66. Sokka,A.-L., Putkonen,N., Mudo,G., Pryazhnikov,E., Reijonen,S., Khiroug,L.,
40 Belluardo,N., Lindholm,D. and Korhonen,L. (2007) Endoplasmic reticulum stress
41 inhibition protects against excitotoxic neuronal injury in the rat brain. *J Neurosci*, **27**,
42 901–908.
- 43
44 67. Portillo,J.-A.C., Okenka,G., Kern,T.S. and Subauste,C.S. (2009) Identification of
45 primary retinal cells and ex vivo detection of proinflammatory molecules using flow
46 cytometry. *Mol Vis*, **15**, 1383–1389.
- 47
48
49
50
51
52
53
54
55
56
57
58
59
60

Legends to figures

Figure 1. Calpain and Aif activation in retinas bearing mutation in the *Rho* gene. (A)

Immunoblot of total protein extracts (PN9 for *Rho*^{+/+} and *P23H*^{Tg}; PN16 for *Rho*^{+/-} and *Rho*^{P23H/-}; PN45 for *Rho*^{+/+} and *Rho*^{-/-}) with an anti- α -II-spectrin antibody is shown. All mutant retinas manifest an increased intensity of the 145 kDa band (arrow). Retinas expressing the P23H mutation also show fragments of α -II-spectrin at 120 kDa (asterisk) consistent with activation of caspases. The immunoblot was normalized with anti-actin antibodies (lower panel). MW: molecular weight markers are shown in kDa. (B) Histogram representing the percentages of cells co-labeled with TUNEL and with the calpain activity assay. (C) Confocal images showing co-localization (yellow, arrows) of Aif (red) and TUNEL (green) inside nuclei of *P23H*^{Tg} retinas at PN9, *Rho*^{P23H/-} retinas at PN16, and *Rho*^{-/-} retinas at PN45. IS = inner segment (containing photoreceptor cytoplasm and mitochondria); ONL= outer nuclear layer; INL = inner nuclear layer. Scale bar: 50 μ m (D) Histogram representing percentages of cells co-labeled with TUNEL and with the anti-Aif antibody. (E) Immunoblots of nuclear enriched extracts from *Rho*^{+/+} PN10 and *P23H*^{Tg} retinas at PN8, PN9 and PN10 (8, 9 10 in the figure), from *Rho*^{+/-} PN20 and *Rho*^{P23H/-} retinas at PN12, PN16 and PN20 (12, 16, 20 in the figure), from *Rho*^{+/+} PN30 and *Rho*^{-/-} retinas at PN30, PN45 and PN60 (30, 45, 60 in the figure) using an anti-Aif antibody. Immunoblots were normalized with anti-histone H3 antibodies (lower panels). MW: molecular weight markers are shown in kDa.

Figure 2. Neuroprotective effects of calpastin peptide treatment. (A) Total protein

extracts from mouse retinas were analyzed by immunoblot at the age of PN10 for *P23H*^{Tg}, PN16 for *Rho*^{P23H/-} and PN45 for *Rho*^{-/-} with an anti- α -II-spectrin antibody and in age-matched controls (*Rho*^{+/+} PN10; *Rho*^{+/-} PN16; *Rho*^{+/+} PN45). The reduction of the 145 kDa

1
2
3 fragment resulting from calpain cleavage (arrow) in calpastatin peptide (CS) treated retinas
4
5 when compared to vehicle treated control retinas (mock) confirmed the inhibition of calpain
6
7 activation by CS. The immunoblot was normalized with anti-actin antibodies (lower panel).
8
9 MW: molecular weight markers are shown in kDa. (B) Histogram with percentages of
10
11 photoreceptors co-labeled with TUNEL and the calpain activity assay, as detected *in situ*
12
13 with a fluorescent calpain substrate, indicates a significant reduction of dying cells
14
15 activating calpains after treatment with CS in all models. (C) Immunoblot of nuclear protein
16
17 extracts shows reduced nuclear translocation of Aif in CS treated samples. The
18
19 immunoblot was normalized with anti-Histone H3 antibodies (lower panel). MW: molecular
20
21 weight markers are shown in kDa. (D) Histogram with percentages of photoreceptors co-
22
23 labeled with TUNEL and nuclear localized Aif reveals a reduction of dying cells activating
24
25 Aif after treatment with CS in all models. (E) Histogram with percentages of TUNEL-
26
27 labeled photoreceptors shows a reduction of photoreceptor cell death after treatment with
28
29 CS. *** $P \leq 0.001$; * $P \leq 0.05$ Student's t-test comparing treated retinas (white bars) with the
30
31 corresponding mock treated controls (gray bars).
32
33
34
35
36

37 **Figure 3. Time course of ER-stress activation in P23H^{Tg}.** Ire1 and Perk pathway
38
39 activations were analyzed in *Rho*^{+/+} and *P23H^{Tg}* retinas at PN8, PN9 and PN10 (8, 9 10 in
40
41 figure). (A) Immunoblot of total protein extracts shows phosphorylation/activation of Ire1
42
43 (phospho-Ire1 antibody) in the mutant retina at PN8, PN9 and PN10, the last at a reduced
44
45 level. The immunoblot was normalized using anti-actin antibodies (lower panel). MW:
46
47 molecular weight markers are shown in kDa. (B) RT-PCR with primers specific for the
48
49 spliced form of *Xbp1* (*sXbp1*) confirmed activation of the Ire1 pathway in PN8 and PN9
50
51 mutant retinas. RT-PCR was normalized with primers specific for *S26*. MW=molecular
52
53 weight marker showing DNA fragments every 100 bp starting from the lower band at 100
54
55 bp. (C) Immunofluorescence analysis of retinas at PN9 with anti-phospho-Ire antibodies
56
57
58
59
60

1
2
3 (red in the inner segment, containing the cytoplasm of photoreceptor cells, is indicated by
4
5 an arrow) confirmed activation of the Ire1 pathway in the photoreceptor cells also labeled
6
7 by TUNEL (green). Nuclei are stained with DAPI (blue). Scale bar: 20 μ m. (D) Immunoblot
8
9 of total protein extracts shows phosphorylation/activation of Perk (phospho-Perk antibody)
10
11 in the mutant retina at all tested time points. The immunoblot was normalized using anti-
12
13 Perk antibodies to visualize total Perk protein (lower panel) and to be compared to the
14
15 activated-phosphorylated form shown in the upper panel. MW: molecular weight markers
16
17 are shown in kDa. (E) Immunoblot shows phosphorylation of Eif2 α in the mutant retina at
18
19 all tested time points. The immunoblot was normalized using anti-Eif2 α antibodies to
20
21 visualize total Eif2 α protein (lower panel). MW: molecular weight markers are shown in
22
23 kDa. (F) Immunofluorescence analysis of retinas at PN10 with antibodies anti-P-Perk (red
24
25 in the inner segment, containing the cytoplasm of photoreceptor cells, is indicated by an
26
27 arrow) confirmed activation of the Perk pathway in the photoreceptor cells also labeled by
28
29 TUNEL (green). Nuclei are stained with DAPI (blue). Scale bar: 20 μ m. IS = inner segment
30
31 (containing photoreceptor cytoplasm and mitochondria); ONL= outer nuclear layer; INL =
32
33 inner nuclear layer; GCL=ganglion cell layer.

34
35
36
37
38
39
40
41
42
43 **Figure 4. Time course of ER-stress activation in $Rho^{P23H/-}$.** Ire1 and Perk pathway
44
45 activations were analyzed in in $Rho^{P23H/-}$ retinas at PN12, PN16 and PN28 (12, 16, 28 in
46
47 figure) and compared to $Rho^{+/-}$ retinas at the same ages. (A) Immunoblot of total protein
48
49 extracts shows phosphorylation/activation of Ire1 (phospho-Ire1 antibody) in the mutant
50
51 retina at all analyzed time points. The immunoblot was normalized using anti-actin
52
53 antibodies (lower panel). MW: molecular weight markers are shown in kDa. (B) RT-PCR
54
55 with primers specific for the spliced form of *Xbp1* (*sXbp1*) confirmed activation of the Ire1
56
57
58
59
60

1
2
3 pathway in mutant retinas. RT-PCR was normalized with primers specific for S26.
4
5 MW=molecular weight marker showing DNA fragments every 100 bp starting from the
6
7 lower band at 100 bp. (C) Immunofluorescence analysis of retinas at PN16 with anti-
8
9 phospho-Ire antibodies (red in the inner segment, containing the cytoplasm of
10
11 photoreceptor cells, is indicated by an arrow) confirmed activation of the Ire1 pathway in
12
13 the photoreceptor cells also labeled by TUNEL (green). Nuclei are stained with DAPI
14
15 (blue). Scale bar: 20 μ m. (D) Immunoblot of total protein extracts shows
16
17 phosphorylation/activation of Perk (phospho-Perk antibody) in the mutant retina at all
18
19 tested time points. The immunoblot was normalized using anti-Perk antibodies to visualize
20
21 total Perk protein (lower panel) and to be compared to the activated-phosphorylated form
22
23 shown in the upper panel. MW: molecular weight markers are shown in kDa. (E)
24
25 Immunoblot shows phosphorylation of Eif2 α in the mutant retina at all tested time points.
26
27 The immunoblot was normalized using anti-Eif2 α antibodies to visualize total Eif2 α protein
28
29 (lower panel). MW: molecular weight markers are shown in kDa. (F) Immunofluorescence
30
31 analysis of retinas at PN16 with antibodies anti-phospho-Perk (red in the inner segment,
32
33 containing the cytoplasm of photoreceptor cells, is indicated by an arrow) confirmed
34
35 activation of the Perk pathway in the photoreceptor cells also labeled by TUNEL (green).
36
37 Nuclei are stained with DAPI (blue). Scale bar: 20 μ m. IS = inner segment (containing
38
39 photoreceptor cytoplasm and mitochondria); ONL= outer nuclear layer; INL = inner nuclear
40
41 layer; GCL=ganglion cell layer.
42
43
44
45
46
47
48
49
50
51
52
53
54
55
56
57
58
59
60

Figure 5. Neuroprotective effects of salubrinal and calpastatin treatments. Mice were treated either with salubrinal (SAL) or calpastatin peptide (CS) or with salubrinal and calpastatin peptide together (CS+SAL). Protein extracts from retinas treated with drugs or

1
2
3 treated with vehicle only (mock) were analyzed at the age of PN9 for $P23H^{Tg}$ and PN16 for
4 $Rho^{P23H/-}$. **(A-B)** Immunoblots of total protein extracts show increased phosphorylated Ire1
5 (upper panels) after treatment with SAL and CS+SAL in $P23H^{Tg}$ **(A)** and in $Rho^{P23H/-}$ **(B)**
6 retinas. No effect on Ire1 phosphorylation was observed after treatment with CS only.
7 Immunoblots were normalized using anti-actin antibodies (lower panel). **(C-D)** RT-PCR
8 using primers specific for the spliced form of *Xbp1* (*sXbp1*) confirms activation of the Ire1
9 pathway after treatment with SAL and CS+SAL in $P23H^{Tg}$ **(C)** and in $Rho^{P23H/-}$ **(D)** retinas.
10 No effect on *Xbp1* splicing was observed after treatment with CS only. RT-PCR reactions
11 were normalized with primers specific for *S26*. **(E-F)** Immunoblots of total protein extracts
12 show no significant change of phosphorylated Perk (upper panels) in $P23H^{Tg}$ **(E)** and in
13 $Rho^{P23H/-}$ **(F)** retinas after treatments. The immunoblots were normalized using anti-Perk
14 antibodies (lower panels). **(G-H)** Immunoblots of total protein extracts show increased
15 phosphorylated Eif2 α (upper panels) after treatment with SAL and CS+SAL in $P23H^{Tg}$ **(G)**
16 and in $Rho^{P23H/-}$ **(H)** retinas. Immunoblots were normalized using anti-Eif2 α antibodies
17 (lower panel). **(I-J)** Immunoblots of nuclear protein extracts show reduced nuclear
18 translocation of Aif (upper panels) in $P23H^{Tg}$ **(I)** and in $Rho^{P23H/-}$ **(J)** retinas after
19 treatments. Immunoblots were normalized using anti-Histone H3 antibodies (lower panel).
20 **(K-L)** Immunoblots on total protein extracts show increased Bip/Grp79 (upper panels) after
21 treatment with SAL and CS+SAL in $P23H^{Tg}$ **(K)** and in $Rho^{P23H/-}$ **(L)** retinas. No effect on
22 Bip/Grp79 levels was observed after treatment with CS only. Immunoblots were
23 normalized using anti-actin antibodies (lower panel). **(M)** Graph representing the
24 percentages of TUNEL⁺ photoreceptors in $P23H^{Tg}$ (dashed bars) and in $Rho^{P23H/-}$ (gray
25 bars) after treatments with either SAL or CS or CS+SAL. A significant reduction of cell
26 death was observed in all treated retinas when compared to retinas treated with vehicle
27 only (mock). **(N)** Graph representing the percentages of dying photoreceptors activating

1
2
3 calpains (Calpain activity⁺/TUNEL⁺) in *P23H^{Tg}* (dashed bars) and in *Rho^{P23H/-}* (gray bars)
4
5 after treatments with either SAL or CS or CS+SAL. A significant reduction of calpain
6
7 activation in dying cells was detected in *P23H^{Tg}* and *Rho^{P23H/-}* retinas only after treatments
8
9 with CS when compared to retinas treated with vehicle only (mock). (O) Graph
10
11 representing the percentages of dying photoreceptors with nuclear localized Aif
12
13 (Aif⁺/TUNEL⁺) in *P23H^{Tg}* (dashed bars) and in *Rho^{P23H/-}* (gray bars) after treatments with
14
15 either SAL or CS or CS+SAL. A significant reduction of Aif activation in dying cells was
16
17 detected in all treated retinas expressing P23H mutant Rho when compared to retinas
18
19 treated with vehicle only (mock). *** $P \leq 0.001$; ** $P \leq 0.01$; * $P \leq 0.05$ t-Student comparing
20
21 treated retinas with the corresponding mock controls. MW: molecular weight markers are
22
23 shown in kDa.
24
25
26
27

28 **Figure S1. Characterization of murine mutant Rho models.** (A) Time course analysis of
29 photoreceptor cell death in *P23H^{Tg}*, *Rho^{P23H/-}*, and *Rho^{-/-}* mutant retinas by TUNEL assay.
30 Peak of cell death was postnatal day 9 (PN9) in *P23H^{Tg}*, PN16 in *Rho^{P23H/-}*, and PN45 in
31
32 *Rho^{-/-}*. (B) Immunoblots using anti-Rho antibody (1D4, Sigma) of total protein extracts from
33 retinas of *Rho^{P23H/-}* compared to *Rho^{+/-}* and *Rho^{-/-TgP23H}* (*P23H^{Tg}* bred with *Rho^{-/-}* to analyze
34 only the mutant transgenic allele) compared to wild type *Rho^{+/+}*. Rho monomers are
35 indicated by an open arrow. Blots were normalized with an anti-recoverin antibody (lower
36 panel, Rec), a protein expressed in photoreceptors, to take into account on-going rod cell
37 death at the analyzed time points. MW: molecular weight markers are shown in kDa. (C)
38
39 Confocal images of immunofluorescence analyses of *Rho^{+/+}* and *P23H^{Tg}* retinas at PN10
40 and *Rho^{+/-}* and *Rho^{P23H/-}* retinas at PN16 labeled with the anti-Rho antibody (green) and
41
42 TUNEL (red). Wild type Rho accumulates in the inner segment (IS) at PN10 and in the
43
44 outer segment (OS) of the more mature retina at PN16 but mutant P23H accumulates
45
46 intracellularly and is retained in the inner segment. Dying cells labeled with TUNEL are
47
48
49
50
51
52
53
54
55
56
57
58
59
60

1
2
3 detectable only in P23H expressing retinas. Scale bars: 75 μ m. **(D)** Analyses of calpain
4 activity (blue) and TUNEL (red) of *Rho*^{+/+} and *P23H*^{Tg} retinas at PN10, *Rho*^{+/-} and *Rho*^{P23H/-}
5 retinas at PN16 and *Rho*^{+/+} and *Rho*^{-/-} retinas at PN45. Arrows indicate cells co-labeled by
6 TUNEL and the calpain activity assay; arrowheads indicate cells labeled only by the
7 calpain activity assay. OS= outer segment; IS = inner segment (containing photoreceptor
8 cytoplasm and mitochondria); ONL= outer nuclear layer; INL = inner nuclear layer. **(E-G)**
9
10 Confocal sections of *P23H*^{Tg} **(E)**, *Rho*^{P23H/-} **(F)** and *Rho*^{-/-} **(G)** retinas stained with anti-Aif
11 (red) and TUNEL (green) confirming nuclear translocation of Aif in dying cells (arrows).
12 Some TUNEL positive cells do not show nuclear translocation of Aif (arrowhead). Merge:
13 merged images of the red, green and blue channels. Nuclei were stained with DAPI (blue).
14
15
16
17
18
19
20
21
22
23
24
25

26 **Figure S2. Analyses of Calcium in murine mutant Rho photoreceptors.** **(A)** Flow
27 cytometry characterization of the cell population dissociated from a PN16 *Rho*^{+/-} retina.
28 The cell population and the rod photoreceptor cells labeled with the 1D4 anti-Rho antibody
29 (Q2 gate) show a bimodal pattern as previously reported (67). This photoreceptor
30 population was gated for all subsequent studies. **(B)** Histogram representing percentages
31 of cells with high levels of Ca²⁺. A significant increase was observed in mutant retinas (***)
32 *P*≤0.001). **(C-E)** Flow cytometry outcomes of calcium labeling with Fluo-4 AM
33 (fluorescence intensity on the Y axis) in *P23H*^{Tg} and *Rho*^{+/+} at PN10 **(C)**; in *Rho*^{P23H/-} and
34 *Rho*^{+/-} at PN16 **(D)** and in *Rho*^{-/-} and *Rho*^{+/+} at PN45 **(E)**. Gates applied measure the cell
35 percentages with high level of Ca²⁺.
36
37
38
39
40
41
42
43
44
45
46
47
48

49 **Figure S3. Quantification of experiments shown in figure 5.** Mice were treated either
50 with salubrinal (SAL, green bars) or calpastatin peptide (CS, blue bars) or with salubrinal
51 and calpastatin peptide together (CS+SAL, black bars). Protein extracts from retinas
52 treated with drugs or treated with vehicle only (mock, white bars) were analyzed at the age
53
54
55
56
57
58
59
60

of PN9 for $P23H^{Tg}$ and PN16 for $Rho^{P23H/-}$. **(A-B)** Quantifications of western blots of total protein extracts show significant increase of phosphorylated Ire1 after treatment with SAL and CS+SAL in $P23H^{Tg}$ **(A)** or in $Rho^{P23H/-}$ **(B)** retinas. No effect on Ire1 phosphorylation was observed after treatments with CS only. **(C-D)** Quantifications of RT-PCR analyzing the spliced form of *Xbp1* (*sXbp1*) confirm activation of the Ire1 pathway after treatment with SAL and CS+SAL in $P23H^{Tg}$ **(C)** or in $Rho^{P23H/-}$ **(D)** retinas. No effect on *Xbp1* splicing was observed after treatment with CS only. **(E-F)** Quantifications of immunoblots of total protein extracts show no significant change of phosphorylated Perk in either $P23H^{Tg}$ **(E)** or $Rho^{P23H/-}$ **(F)** retinas. **(G-H)** Quantifications of immunoblots of total protein extracts show significant increase of phosphorylated Eif2 α after treatment with SAL and CS+SAL in $P23H^{Tg}$ **(G)** and in $Rho^{P23H/-}$ **(H)** retinas. No effect on Eif2 α phosphorylation was observed after treatment with CS only. **(I-J)** Quantifications of immunoblots of nuclear protein extracts show significantly reduced nuclear translocation of Aif after treatment with SAL or CS in $P23H^{Tg}$ **(I)** and in $Rho^{P23H/-}$ **(J)** retinas. **(K-L)** Quantifications of immunoblots of total protein extracts show significant increase of Bip/Grp79 after treatment with SAL and CS+SAL in $P23H^{Tg}$ **(K)** and in $Rho^{P23H/-}$ **(L)** retinas. No effect on Bip/Grp79 levels was observed after treatment with CS only. *** $P \leq 0.001$; ** $P \leq 0.01$; * $P \leq 0.05$ t-Student comparing treated retinas with the corresponding controls (white bars).

Figure S4. Histological analysis of treated retinas. **(A, C, E)** Histological analysis by Hematoxylin-Eosin staining of $P23H^{Tg}$ **(A)**, $Rho^{P23H/-}$ **(C)** and $Rho^{-/-}$ **(E)** mutant retinas after treatments with vehicle only (mock) or with salubrinal (SAL) or calpastatin peptide (CS) or with calpastatin peptide and salubrinal together (CS+SAL). ONL= outer nuclear layer; INL = inner nuclear layer; GCL= ganglion cell layer. Scale bar: 100 μ m. **(B, D)** Immunofluorescence analysis of RHO protein (green) in $P23H^{Tg}$ **(B)** and $Rho^{P23H/-}$ **(D)** retinas after treatments with vehicle only (mock) or with salubrinal (SAL) or calpastatin

1
2
3
4
5
6
7
8
9
10
11
12
13
14
15
16
17
18
19
20
21
22
23
24
25
26
27
28
29
30
31
32
33
34
35
36
37
38
39
40
41
42
43
44
45
46
47
48
49
50
51
52
53
54
55
56
57
58
59
60

peptide (CS) or with calpastatin peptide and salubrinal together (CS+SAL). Sections were co-stained with the anti-PERK antibody (red) identifying the ER. Scale bar: 20µm.

For Peer Review

Abbreviations

Aif: apoptosis-inducing factor

ER: endoplasmic reticulum

ERAD: ER-associated degradation

RHO: human Rhodopsin

Rho: murine Rhodopsin

RP: retinitis pigmentosa

UPR: unfolded protein response

For Peer Review

1
2
3
4
5
6
7
8
9
10
11
12
13
14
15
16
17
18
19
20
21
22
23
24
25
26
27
28
29
30
31
32
33
34
35
36
37
38
39
40
41
42
43
44
45
46
47
48
49
50
51
52
53
54
55
56
57
58
59
60

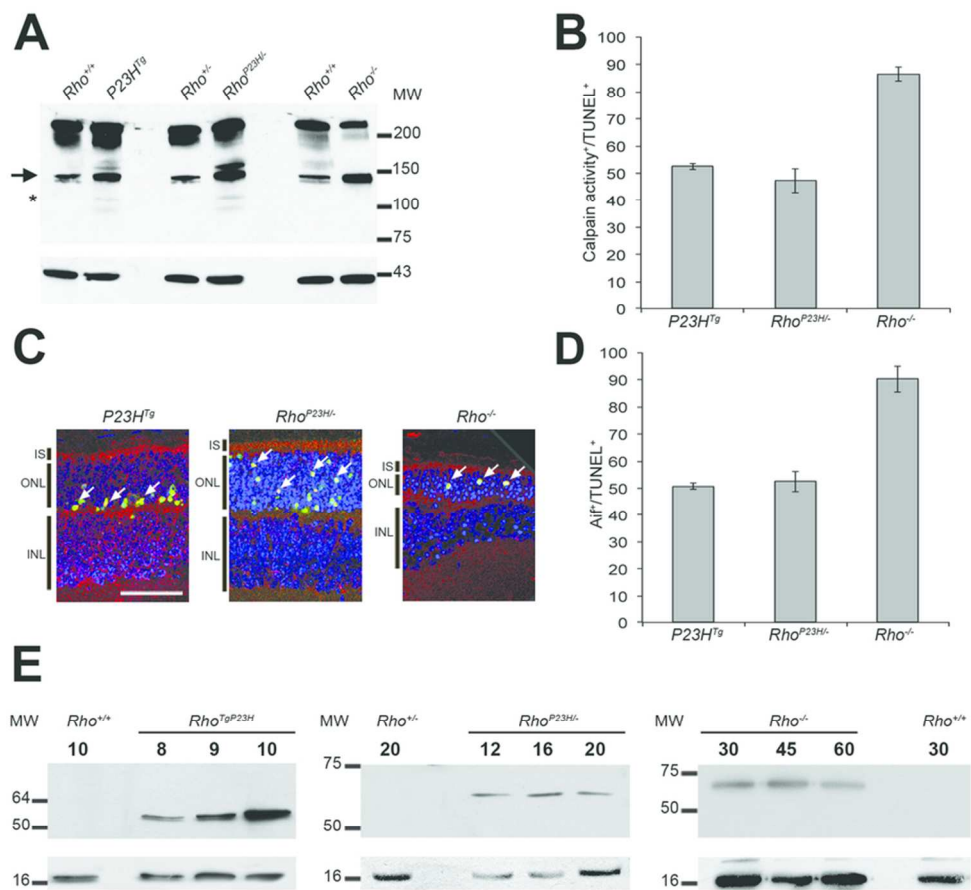


Figure 1
80x75mm (300 x 300 DPI)



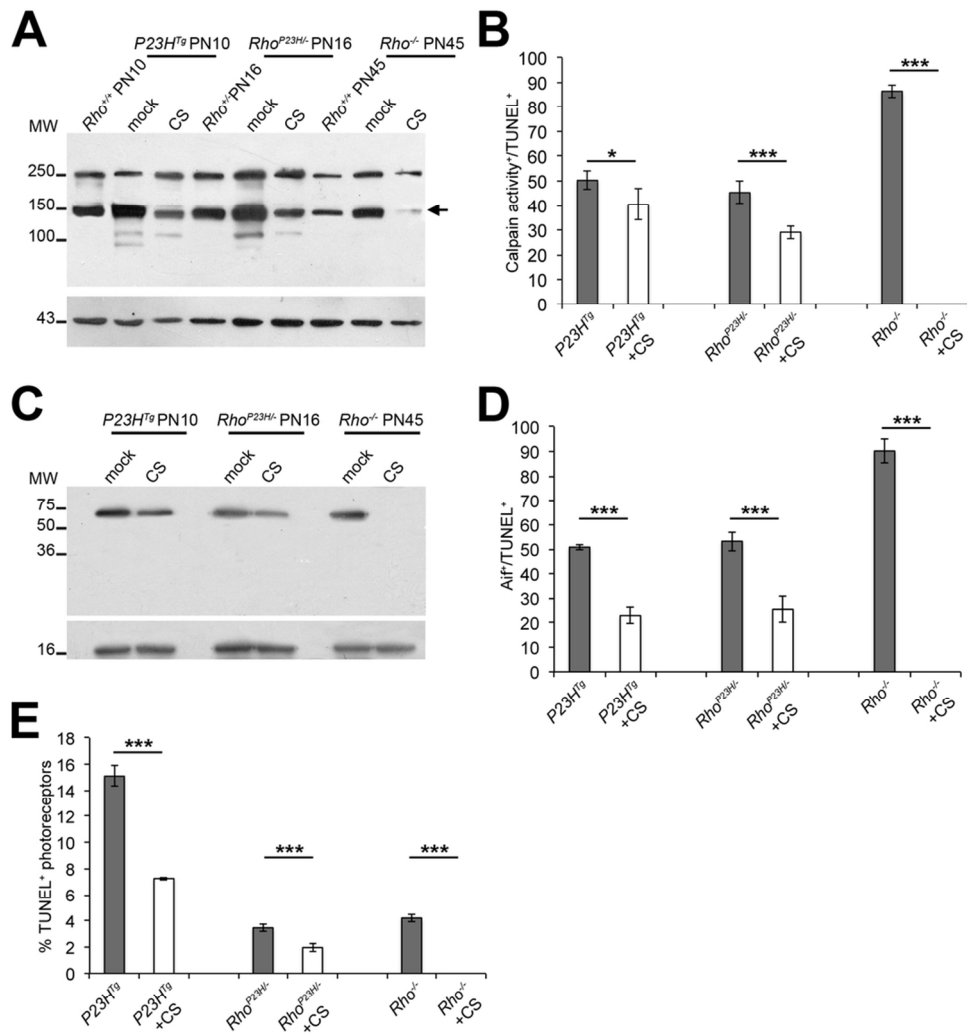


Figure 2
93x101mm (300 x 300 DPI)

1
2
3
4
5
6
7
8
9
10
11
12
13
14
15
16
17
18
19
20
21
22
23
24
25
26
27
28
29
30
31
32
33
34
35
36
37
38
39
40
41
42
43
44
45
46
47
48
49
50
51
52
53
54
55
56
57
58
59
60

1
2
3
4
5
6
7
8
9
10
11
12
13
14
15
16
17
18
19
20
21
22
23
24
25
26
27
28
29
30
31
32
33
34
35
36
37
38
39
40
41
42
43
44
45
46
47
48
49
50
51
52
53
54
55
56
57
58
59
60

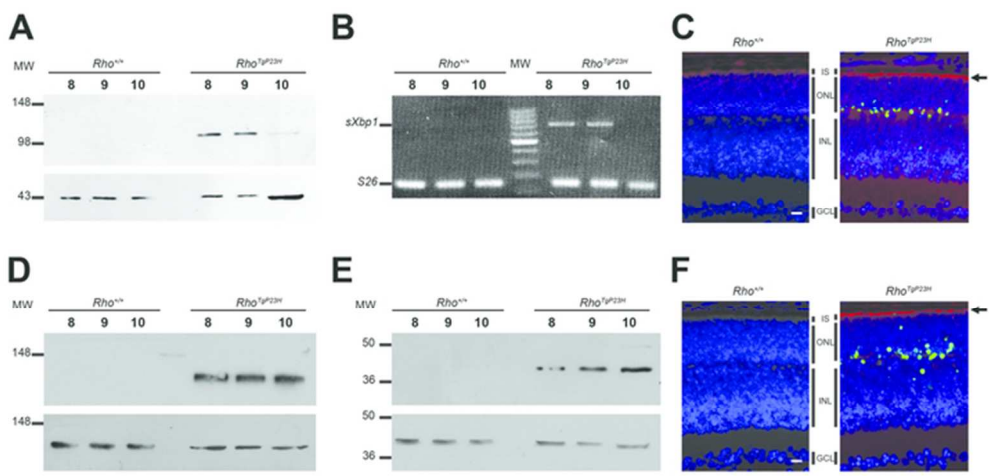


Figure 3
61x30mm (300 x 300 DPI)

Peer Review

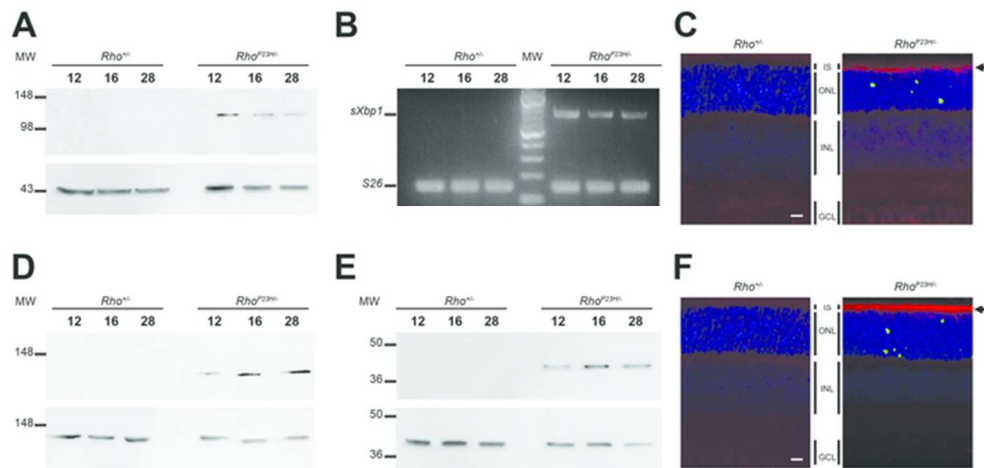
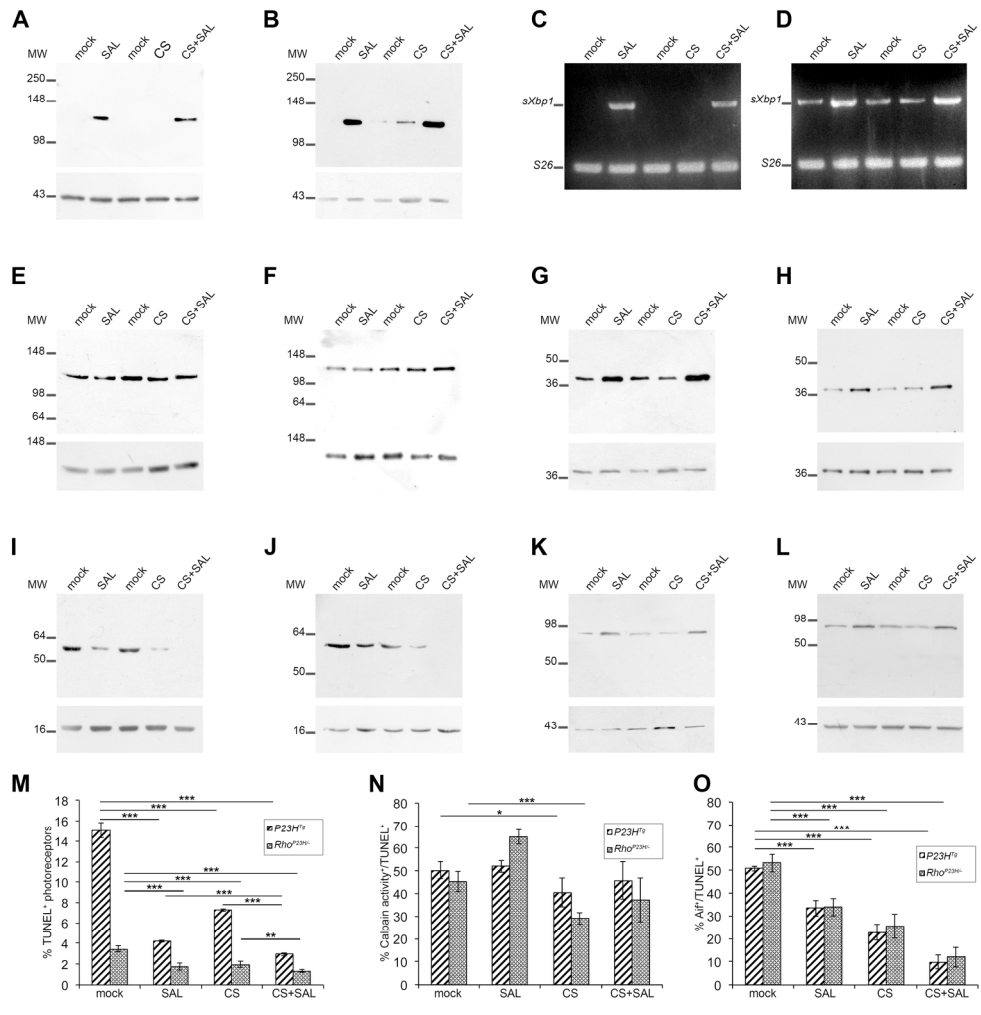


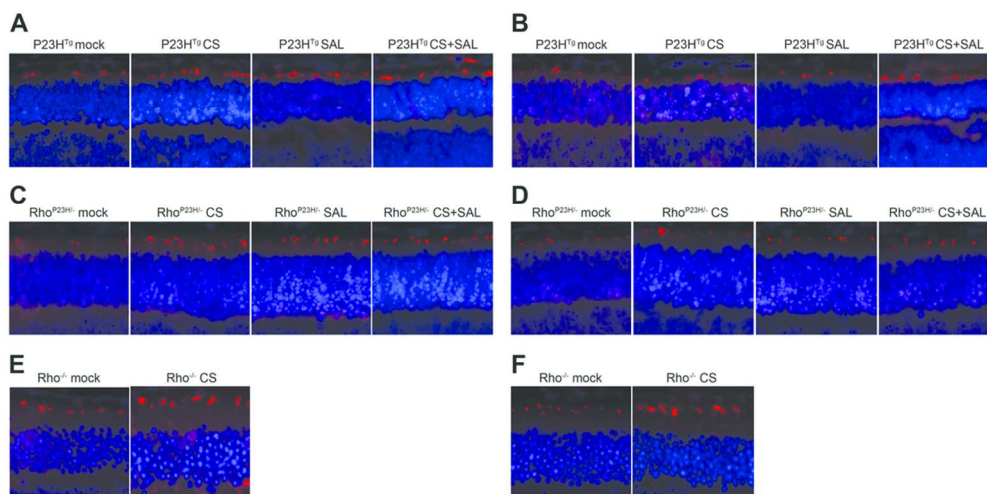
Figure 4
61x30mm (300 x 300 DPI)

Peer Review

1
2
3
4
5
6
7
8
9
10
11
12
13
14
15
16
17
18
19
20
21
22
23
24
25
26
27
28
29
30
31
32
33
34
35
36
37
38
39
40
41
42
43
44
45
46
47
48
49
50
51
52
53
54
55
56
57
58
59
60



186x192mm (300 x 300 DPI)



Cone analysis after treatments: Retina sections were analyzed by immunofluorescence with anti-OPN1MW (M cone opsin) (A, C, E) or anti-OPN1SW (S cone opsin) (B, D, F), shown in red, in mock treated P23H^{Tg} (A-B), Rho^{P23H} (C-D), Rho^{-/-} (E-F) mice or treated with calpastatin peptide (CS), salubrinal (SAL) or calpastatin peptide and salubrinal (CS+SAL).

98x57mm (300 x 300 DPI)

er Review

1
2
3
4
5
6
7
8
9
10
11
12
13
14
15
16
17
18
19
20
21
22
23
24
25
26
27
28
29
30
31
32
33
34
35
36
37
38
39
40
41
42
43
44
45
46
47
48
49
50
51
52
53
54
55
56
57
58
59
60